ELECTROMAGNETIC FORM FACTORS OF N* RESONANCES AND THEIR DETERMINATION FROM PION ELECTROPRODUCTION

R.C.E. DEVENISH
Deutsches Elektronen-Synchrotron DESY, Hamburg

D.H. LYTH
Department of Physics, University of Lancaster, Lancaster, U.K.

We show how N* electromagnetic form factors can be parameterised in a simple way to take account of their known behaviour at threshold. Using such form factors and Breit-Wigners to represent the final-state interaction we calculate the imaginary parts of the invariant amplitudes for the process $eN \to eN\pi$, the real parts are calculated from fixed t dispersion relations. The complete amplitudes are then fit to the coincidence data in the resonance region $(0 < |\lambda^2| < 1.0 \text{ GeV}^2; w < 2 \text{ GeV})$ in order to determine the form factor parameters. Results are presented for the λ^2 dependence of the resonant multipoles and in particular we find stable results for the $P_{11}(1434)$, $S_{11}(1505)$, $D_{13}(1520)$, $F_{15}(1688)$ and $F_{37}(1940)$. A critical discussion is given of the effect of theoretical uncertainties on the results. We use our results to calculate the helicity asymmetry A on the resonant peaks seen in eN scattering and find that on the 2nd and 3rd peaks A changes sign in the vicinity of $\lambda^2 \approx -1 \text{ GeV}^2$.

1. Introduction

Inelastic electron scattering has been considered for a long time to be one of the best ways of studying the structure of the nucleon. Although there is a lot of data for the total inelastic cross section in the resonance region, only the properties of the 1st resonance, the $P_{33}(1232)$, are well understood. In the absence of data from polarised targets resonance information could be used to examine Bloom-Gilman duality [1] more fully, for example. The behaviour of the nucleon and N* form factors also provides a very searching test of constituent models [2].

The exclusive process of single pion electroproduction $eN \to eN\pi$ is one of the most fruitful sources of information on resonance structure. The properties of the $P_{33}(1232)$ have been largely determined by studying coincidence data on $ep \to ep\pi^0$. Some coincidence data exist at higher energies and a number of explanatory calculations have been made using fixed-t dispersion relation techniques with some success

[3], notable being the extraction of the pion-form factor from data on ep $\rightarrow$ enπ^+ just above the resonance region [4,5].

Recently the situation has improved in two ways which will enable real progress to be made on extracting the detailed behaviour of the N* resonance form factors. The first and obvious one is that a lot more coincidence data on both ep $\rightarrow$ epπ^0 and ep $\rightarrow$ enπ^+ is available in the resonance region and much more can be expected in the next few years. The second is that we now have reliable multipole analyses of photoproduction [6] on which to base an electroproduction analysis.

In this paper we will describe the determination of N* resonance form factors from coincidence data on eN $\rightarrow$ eNπ. Sect. 2 is devoted to the choice of form factors. Sect. 3 describes the method based on the resonance saturation of fixed-t dispersion relations, with special attention to the uncertainties present in such an approach. We give a brief description of the data in sect. 4. The results are given in sect. 5 (numerical details in appendix B) and we conclude with a discussion of the results in sect. 6.

2. Form factors

The subject of the choice of electromagnetic transition form factors for particles with spin has a long history [7]. We will be guided by two principles, convenience and analyticity — in particular the avoidance of unnecessary kinematic singularities. Convenience in being able to perform simple partial wave expansions and a simple connection to photoproduction speaks immediately of multipoles or helicity elements. We choose to use multipoles $E_{l\pm}$, $M_{l\pm}$ (transverse) and $S_{l\pm}$ (scalar).

Considered as functions of λ^2, (photon mass)^2, the multipole amplitudes will have kinematic singularities and be subject to certain constraints. The problem of how to find kinematic singularity free form factors for the coupling of a photon to two particles of spin s and s' has been considered in detail by Theis and Hertel [8], and the special case of the γNΔ form factors has been considered by Jones and Scadron [9]. The threshold behaviour and constraints that we describe below agree with the above results and we sketch in appendix A how the results can also be derived from the invariant amplitude decomposition for pion electroproduction.

Define

$$\alpha_{l+} = (lM_{l+} + E_{l+})/(l + 1) \,,$$

$$\beta_{l+} = (M_{l+} - (l + 2)E_{l+})/(l + 1) \,, \tag{1}$$

and $\phi_\pm^2 = 1 - \lambda^2/m_\pm^2$ where $m_\pm = m^* \pm m$ (m^* is the N* resonance mass, m the nucleon mass). Then if

$$\alpha_{l+} = \phi_-^l \phi_+^{l+1}\bar\alpha_{l+} \,,$$

$$\beta_{l+} = \phi_-^l \phi_+^{l-1}\bar\beta_{l+} \,,$$

$$S_{l+} = \phi_-^{l+1}\phi_+^l \bar{s}_{l+} \ . \tag{2}$$

$\bar{\alpha}, \bar{\beta}$ and $\bar{s}$ will be free of kinematic singularities. There are in addition the constraints:

$$\frac{k_0}{k} S_{l+} \to E_{l+} \qquad \text{as} \qquad \phi_\pm \to 0 \ , \tag{3}$$

where k_0 and k are the virtual photon's energy and three-momentum in the N* rest frame. For $l = 0$ we have an exception,

$$E_{0+} = \phi_+ \bar{E}_{0+} \ , \qquad S_{0+} = \phi_- \phi_+^2 \bar{s}_{0+} \ , \tag{4}$$

and the constraint (3) only applies as $\phi_- \to 0$. For the other multipoles (E_{l-} etc.) we can use Macdowell symmetry [10], in fact from the definition of α and β we have simply that: (note that, $\phi_\pm(-m^*) = \phi_+(m^*)$)

$$E_{l+1-}(m^*) = \beta_{l+}(-m^*) \ ,$$

$$M_{l+1-}(m^*) = \alpha_{l+}(-m^*) \ ,$$

$$S_{l+1-}(m^*) = S_{l+}(-m^*) \ .$$

Hence

$$E_{l-} = \phi_+^{l-1}\phi_-^{l-2}\bar{E}_{l-} \ ,$$

$$M_{l-} = \phi_+^{l-1}\phi_-^l \bar{M}_{l-} \ ,$$

$$S_{l-} = \phi_+^l \phi_-^{l-1}\bar{s}_{l-} \ . \tag{5}$$

The constraint (3) becomes

$$\frac{k_0}{k} S_{l-} \to (M_{l-} - (l-1)E_{l-})/l \qquad \text{as} \qquad \phi_+ \to 0$$

$$- (l-1)E_{l-}/l \qquad \text{as} \qquad \phi_- \to 0 \ . \tag{6}$$

With the exceptional case

$$\frac{k_0}{k} S_{1-} \to M_{1-} \qquad \text{as} \qquad \phi_+ \to 0 \qquad \text{only} \ .$$

The reduced amplitudes $\bar{\alpha}, \bar{\beta}, \bar{E}, \bar{M}$ and $\bar{s}$ will be analytic functions of λ^2 but because of the large N* mass there will an anomalous threshold cut, in addition to the usual normal threshold cut starting at $4\mu^2$ [11]. In order to calculate the imaginary parts of the amplitudes required as input to the dispersion relations we write for a reduced multipole amplitude,

$$\bar{\alpha} = G_\alpha(\lambda^2) f_\alpha(w, w_R, ...) ,\tag{7}$$

where $G_\alpha(\lambda^2)$ is the form factor defined such that $G(0) = 1$ and f_α takes care of the final state interactions, (in the case of a resonant amplitude f_α will be a Breit-Wigner). We now require to parametrise the $G_\alpha(\lambda^2)$ in such a way so as to respect the analytic structure and yet in a realistic way considering that we have only data in the spacelike region with which to determine the parameters. This we do in the simplest possible way by a product of poles lying on the real λ^2 axis between $2\mu^2$* and m_+^2.

This is intended to be an *effective parametrisation*, to represent the total contribution of the cut including the anomalous piece. We write

$$G_\alpha(\lambda^2) = \prod_{i=1}^{n_\alpha} (1 - \lambda^2/\lambda_i^2)^{-1} ,$$

where

$$\lambda_i^2 = \lambda_1^2 + \frac{i}{n}(\lambda_2^2 - \lambda_1^2) ,\tag{8}$$

λ_1^2 and λ_2^2 being the parameters and $2\mu^2 \leqslant \lambda_1^2 \leqslant \lambda_2^2 \leqslant m_+^2$.

The number of poles required in a given form factor is determined by the angular momentum of the state (i.e. extra poles are required to compensate for the powers of λ^2 that occur in the definitions in eqs. (2) and (5)) and by the asymptotic power n of $(\lambda^2)^{-1}$ required for the resonance contribution to the total cross section. Unfortunately there is very little known about n theoretically. The analysis of deep inelastic scattering data by Bloom and Gilman [1] suggests that at fixed w, $\sigma \sim (\lambda^2)^{-3}$ except perhaps for the 1st resonance peak which may have a faster decrease. Given n we can read off from eqs. (2) and (5) the number of poles in a given form factor. For the transverse multipoles we have

$$n_\alpha = l + \tfrac{1}{2}(n + 1) ,$$

$$n_\beta = l + \tfrac{1}{2}(n - 1) , \qquad \text{for} \qquad j = l + \tfrac{1}{2} ;$$

$$n_E = l + \tfrac{1}{2}(n - 3) ,$$

$$n_M = l + \tfrac{1}{2}(n - 1) , \qquad \text{for} \qquad j = l - \tfrac{1}{2} .\tag{9}$$

(Obviously we can only have n odd). It is interesting to note that precisely this type of form factor emerges from the dual B_5 model of pion electroproduction**.

The scalar multipoles present more of a problem as we now have the threshold

---

* $2\mu^2$ is the approximate lowest value of the anomalous cut on the real axis [11].
** We thank J. Körner [12] for pointing this out to us.

constraints to respect and we have no information from photoproduction. From total cross-section measurements the ratio of scalar to transverse cross sections is known to be small in the resonance region (<20%) [13] and in the scaling region [14]. Again we choose a very simple prescription capable of satisfying these constraints, namely

$$S_{l+}(\lambda^2) = \frac{c k(m^*, \lambda^2)}{(\lambda^2 - a)(\lambda^2 - b)} E_{l+}(\lambda^2) \tag{10}$$

(Similarly for S_{l-} with E_{l+} replaced by $(M_{l-} - (l-1)E_{l-})l^{-1})a$ is taken as an independent parameter in the range $2\mu^2 < a < m_+^2$ and b and c are determined from the constraint equations (3) or (6), to be

$$b = (3m^{*2} + m^2 - a)(1 + a(m_+ m_-)^{-1})^{-1} \, ,$$

$$c = 2m^*(m_+^2 - a)(a - m_-^2)(m_+ m_- + a)^{-1} \, . \tag{11}$$

This form allows S_l to vary between 0 (when $a = m_\pm^2$) and a maximum given by solving the constraint equations with $a = b$. For the exceptional cases we write e.g.,

$$S_{0+} = \frac{c k(m^*, \lambda^2)}{\lambda^2 - a} E_{0+} \, . \tag{12}$$

Where now c and a are constrained only at $\phi_- = 0$. (Similarly for S_{1-} at $\phi_+ = 0$.)

3. Fixed t dispersion relations

The details of the dispersion relations and the kinematic formalism can be found in our earlier papers [3,4,15]. We write fixed t dispersion relations for the Ball [16] invariant amplitudes, only one of which, $B_3^{(-)}$, requires a subtraction. The differences between this and our earlier work are the resonance form factors and the revised photoproduction input.

The contribution of a given resonant multipole j to the invariant amplitude B_i is written as follows

$$\text{Im } B_i(s, t, \lambda^2) = k_{ij}(s, t, \lambda^2) G_j(\lambda^2) \text{ Im } f_j(w, w_R \, ...) \, . \tag{12}$$

The k_{ij} are known kinematic functions. The $G_j(\lambda^2)$ are the form factors described in sect. 2. The function $f_j(w, w_R \, ...)$ represents the decay of the N* into the πN final state. For a given resonance we take f to be the same for all multipoles apart from the normalisation. In fact

$$f_\alpha(w, w_R ...) = \frac{w_R \Gamma(q_R/q)^{l+1}}{s_R - s - iw_R \Gamma} \alpha_0 \ ,$$

$$\Gamma = \Gamma_R(q/q_R)^{2l+1} \left(\frac{q_R^2 + X^2}{q^2 + X^2}\right)^l \ , \tag{14}$$

where w_R, Γ_R are the resonance mass, width; q is the πN c.m. momentum. α_0 is the value of the relevant multipole or combination of multipoles taken from photo-production. X is a parameter set to 0.35 for all resonances*. For the $P_{33}(1232)$ we use

$$\frac{k_R q_R}{kq} M_{1+}(w) = \frac{cM_{1+}(w_R)q_R^3}{(q_R^2 - q^2)(1 + q^2 a^2) - icq^3} \ , \tag{15}$$

where $a^2 = 21.4; c = 4.27; q_R = 0.2254$ (GeV units)** and

$$E_{1+}/M_{1+} = (1.19x - 0.25)e^{-3x} \ , \tag{16}$$

where

$$x = \frac{s - m^2}{2m} - 0.15 \text{ (again GeV units)} \ .$$

(This represents an eyeball fit to the multipole analysis of ref. [18].) We now discuss various sources of uncertainty in the calculation.

(i) *Nucleon form factors.* Apart from G_E^N the nucleon form factors are the best known of the inputs to the calculation. We have used the pole model fit of Felst [19][‡], which gives a good representation of the spacelike data. The data on G_E^N shows it to be small and positive out to $\lambda^2 \approx -0.5$ GeV^2 with large errors. For larger λ^2 a change in sign is not ruled out and we discuss below the possible effect in the first resonance region.

(ii) *Pion form factor.* We use our earlier near ρ dominance form factor m_ρ^2 0.5 GeV^2. (If the mass is allowed to float it always remains within a few percent of this value.)

(iii) *Subtraction function in* $B_3^{(-)}$. This of course only affects the charged channels. We have discussed in ref. [15] how the subtraction function could be calculated in principle using a fixed s dispersion relation. The unknown quantity is an integral over the t channel,

---

* This Breit-Wigner form was used in our earlier calculations with slightly different threshold factors [3,4] and also by Walker [46].

** Parameters determined to fit πN phase-shift data of ref. [17].

‡ We also checked that using the "scaling" fit and $G_E^N = 0$, as in our earlier calculations, makes no difference to the results.

$$I_t(\lambda^2) = \int\limits_{4\mu^2}^{\infty} dt' \, \frac{\operatorname{Im} B_3^{(-)}(s_0, t', \lambda^2)}{t' - t} \,.$$

At $\lambda^2 = 0$ gauge invariance gives a sum rule which allows $I_t(0)$ to be determined from s and u channel information. Our ansatz for $I_t(\lambda^2)$ is simply

$$I_t(\lambda^2) = I_t(0) F_s(\lambda^2) \,, \tag{17}$$

i.e. $F_s(\lambda^2)$ represents an "average" form factor for the t channel contributions, in fact we take $F_s = F_\pi$. Again we have checked the sensitivity of the calculation to this term by putting $F_s = 1$. As we have argued in more detail in ref. [15] the subtraction term is unlikely to be important in the region $|t| < 1.0$ GeV^2, $|\lambda^2| < 1.0$ GeV^2 and this is verified by our results.

(iv) *High-energy contribution.* An important improvement in the photoproduction analysis of DLR [6] was to include an effective high-energy parametrisation, determined directly from high energy data simultaneously with the low-energy fit. A similar method is not possible in electroproduction at present because there is little high-energy data. (The only data above the resonance region is at $w = 2.2$–2.5 GeV and is for forward $ep \to en\pi^+$ [20] and backward $ep \to ep\pi^0$ [21]. The former is dominated by F_π and the latter is outside the t acceptance of the calculation.) It is however important to include an estimate of this term — certainly if the resonance spectrum and couplings of DLR are used. We now have to face the notorious problem of how to continue the transverse only information of photoproduction to electroproduction. We choose to continue the Ball amplitudes as follows

$$B_1(s, t, \lambda^2) = (A(s, t) - 2m\, D(s, t)) F_H(\lambda^2) \,,$$

$$B_2(s, t, \lambda^2) = \tfrac{1}{2}(t + \lambda^2 - \mu^2) B(s, t) F_H(\lambda^2) \,,$$

$$B_3(s, t, \lambda^2) = \tfrac{1}{4}(s - u) B(s, t) F_H(\lambda^2) \,,$$

$$B_5(s, t, \lambda^2) = -\tfrac{1}{2}(t - \mu^2) C(s, t) F_H(\lambda^2) \,,$$

$$B_6(s, t, \lambda^2) = -2D(s, t) F_H(\lambda^2) \,,$$

$$B_8(s, t, \lambda^2) = -C(s, t) F_H(\lambda^2) \,, \tag{18}$$

where $A - D$ are the invariant amplitudes of CGLN [22]. This is a slight modification of the method used in VMD calculations [23] to allow the τp or "Stichel rules" to be respected for the s channel helicity amplitudes [24].

We realise that the above prescription will be wrong in detail. The "high-energy" data referred to above indicates that the cross section is in rough agreement with a ρ pole form factor and this is what we use for $F_H(\lambda^2)$ above.

Again we have checked the sensitivity of the calculation to F_H, see sect. 5. One other detail is that the allowed t range is much larger in electroproduction than in photoproduction [3]. The high-energy amplitudes must be cut off for $|t| \gtrsim 1$ GeV^2 as this is outside the range for which the parameters were determined. We have done this with a smooth cutoff function such that by $|t| = 1.6$ GeV^2 the high-energy amplitudes are reduced by a factor $\frac{1}{3}$ and for $|t| > 2$ GeV^2 the contribution is effectively zero. The parametrisation and parameters of the CGLN photoproduction amplitudes are given in DLR.

(v) *Resonance spectrum.* In principle we take the resonance spectrum of DLR. In practise we have dropped some of the resonances with very small couplings. The criteria for exclusion have been the size of the coupling to $\gamma N \rightarrow \pi N$ and the size of the resonance peak in $\sigma_{total}(\gamma N)$. The details of the couplings, parameters, peak heights etc. are given in table 1, appendix B. We are left with 11 resonances. We discuss further the omitted states in sect. 5.

(vi) *Non-resonant s waves.* These are treated exactly as described in ref. [3]. They are important for the calculation of ep $\rightarrow$ epπ^0. The real parts of the multipoles E_{0+}, S_{0+} are projected out from the dispersion relations saturated with the P_{33} alone. The imaginary parts of these multipoles are then calculated using Watson's theorem and introduced into the dispersion relations.

4. Data

4.1. First resonance region

The first resonance can be seen clearly in the eN total cross section for $0 < |\lambda^2| < 3$ GeV^2 and the cross section has been extensively measured in this range: by fitting a resonance + background to the data the peak cross section has been extracted [25]. By making further assumptions about the background the dominant multipole M_{1+} has been extracted [26]. We have choosen to use the peak height data. The total cross-section data itself could be used but this would be extremely time consuming — also the calculation of the π^+n final state at large t and λ^2 emphasises certain ambiguities as explained in sect. 3.

To determine the small multipoles it is essential to have coincidence data and in fact in the range $0 < |\lambda^2| < 1.5$ GeV^2 there is a reasonable coverage of coincidence data for ep $\rightarrow$ epπ^0 in the form of the coefficients of the s + p wave expansion of the cross section [27]. What is lacking is accurate coincidence data for the charged channel.

4.2. Higher resonance region

We use coincidence data above the 1st resonance (i.e. $w \gtrsim 1.4$ GeV) and up to $w \sim 2$ GeV. We can include the complete experimental angular distribution up to

the 3rd resonance region because in each case the maximum t value required is within the limit given by the double spectral function boundary. This is to be compared with photoproduction where a cut must be made $|t| < 1.0$ GeV^2, which will exclude backward hemisphere data above the 2nd resonance region.

In the charged channel $ep \rightarrow en\pi^+$ we have the following data. Forward energy scans at $\lambda^2 = -0.4$, -0.6 and -1.0 GeV^2 [28,29]. The data at -0.4 shows structure at the 2nd and 3rd peaks and at -1 the 3rd peak can again be seen. The NINA experiment [28] also gives forward θ^* hemisphere cross sections for $1.4 < w$ 1.6 GeV. The data from DESY at -0.6 and -1.0 is part of a large experiment to measure the coincidence cross sections in both $ep \rightarrow en\pi^+$ and $ep \rightarrow ep\pi^0$ in the region of the 2nd and 3rd resonance peaks. Preliminary data for $ep \rightarrow en\pi^+$ has been presented by Behrens [30] for $1.0 > \cos \theta^* > 0.45$ and $1.435 < w < 1.555$ at $\lambda^2 = -0.6$ and -1.0 and further for $1.585 < w < 1.735$ GeV at $\lambda^2 = -1.0$ GeV^2. The data is for $\phi^* \approx 90° \pm 20°$*. The angular dependence of the data agrees with that seen at $\phi^* = 90°$ in the earlier NINA experiment at $\lambda^2 = -0.4$, namely $d\sigma/d\Omega^*$ is more or less flat for $w < 1.5$ and then begins to show the characteristic forward peak. As the angular coverage is small little resonance structure can be seen. At $w \sim 2$ GeV we have included the forward π^+n measurements at $\lambda^2 \approx -0.3$ GeV^2 from CEA [31] and at $\lambda^2 \approx -0.7$ GeV^2 from NINA [32].

In the neutral channel $ep \rightarrow ep\pi^0$ we have the NINA data at $\lambda^2 = -0.4$ and -0.6 GeV^2 in the 2nd resonance region [33]. This data was the subject of an earlier investigation using dispersion relations [3] but there the resonance form factors could only be estimated and no attempt was made to fit to data. The backward energy scans at $\lambda^2 = -0.6$ and -1.0 from the DESY experiment were presented at the Bonn conference [29]. We have also been able to use preliminary unpublished angular distributions for $ep \rightarrow ep\pi^0$ at $\lambda^2 = 1.0$ for the backward hemisphere in θ^* and $1.375 < w < 1.735$ GeV [34]. At low energies the data shows the characteristic peaking at central θ^* angles seen in the NINA data [33], above 1.6 GeV the distributions are flatter and show evidence for the angular structure of the F_{15}.

We have also included in our fits the peak height data extracted from the ep total cross section [25]. Although this data is somewhat model dependent it is important as it is the only information that we have on the behaviour of the form factors for $|\lambda^2| > 1.0$ GeV^2.

Data we have not explicitly taken in to account is the measurement of the D/H ratio on the 1st, 2nd and 3rd resonance peaks [25]. The 1st peak is consistent with $D/H = 2$ within small errors, independent of $|\lambda^2|$. The 3rd peak is also consistent with no change in D/H with λ^2 within large errors. The 2nd peak shows perhaps a small decrease in D/H as $|\lambda^2|$ increases. In our calculations the neutron to proton ratio of the couplings cannot change with λ^2. There is no reason in principle why it should not but for the sake of simplicity and the lack of any coincidence data for the neutron channel we have ignored this. The affect of such a small change indi-

---

* Using the ϕ^* convention of K. Berkelman [47].

cated by the data will be very small as it will only enter via the crossed channel contribution to the dispersion integral.

Finally in the second resonance region we have used the data on the process $ep \rightarrow ep\eta$ [35]. In photoproduction the cross section is dominated near threshold by the $S_{11}(1505)$ and the angular dependence of the electroproduction results also indicates s wave dominance. We use the data in the form of the S_{11} peak in the ep total cross section [2]. The surprising feature of this data is the slow decrease of the cross section. The importance of this data will be discussed further in sect. 5.

5. Results

In our earlier investigations of dispersion calculations in electroproduction it was clear that the higher resonances play a very small role in the first resonance region. Our procedure has been to investigate the first resonance region using only the $N + \Delta + s$ wave contributions. When the P_{33} form factor has been determined we fix the value in the fits to the higher resonance regions. Because the coverage of the higher energy data in angle, energy and λ^2 is not uniform we have minimised $(\Sigma \chi^2)/N$ for all data but rather the average of this quantity over blocks of data at a given λ^2, for a given channel and energy range. We have also treated the forward energy scan at $\lambda^2 = -0.4$ in $\pi^+ n$ as a separate block; otherwise this structure tends to be ignored.

5.1. 1st resonance region

In order to accommodate the data in the 1st resonance region we must make a slight modification to our treatment of the scalar multipole S_{1+}. Our ansatz described in sect. 2 is in broad agreement with the data in the sense that both E_{1+} and S_{1+} are small ($<10\% M_{1+}$). However, it can be deduced almost directly from the coefficient data [27] that E_{1+} is smaller than S_{1+}. E_{1+} also has a non resonant energy dependence in photoproduction [18]. For S_{1+} we use the following simple ansatz

$$S_{1+}(\lambda^2) = \frac{-0.1 \ k(m^*, \lambda^2)}{(\lambda^2 - a)} M_{1+}(\lambda^2) . \tag{19}$$

a is a free parameter in the range $2\mu^2 < a < m_+^2$. The sign has been fixed to agree with the coefficient data (see fig. 1 – D_1). Obviously a more complicated parametrisation could be used to incorporate the threshold relation as well. The parametrisation of E_{1+} and M_{1+} has been given in sect. 3. In our approach of resonance saturation of the fixed-t dispersion relations we cannot expect a priori to satisfy Watson's theorem. We have explained briefly in sect. 3 how we solve this problem approximately for the non-resonant s-waves. We have also shown in ref. [3] how with a good representation of the imaginary part of the resonant contribution to M_{1+} the
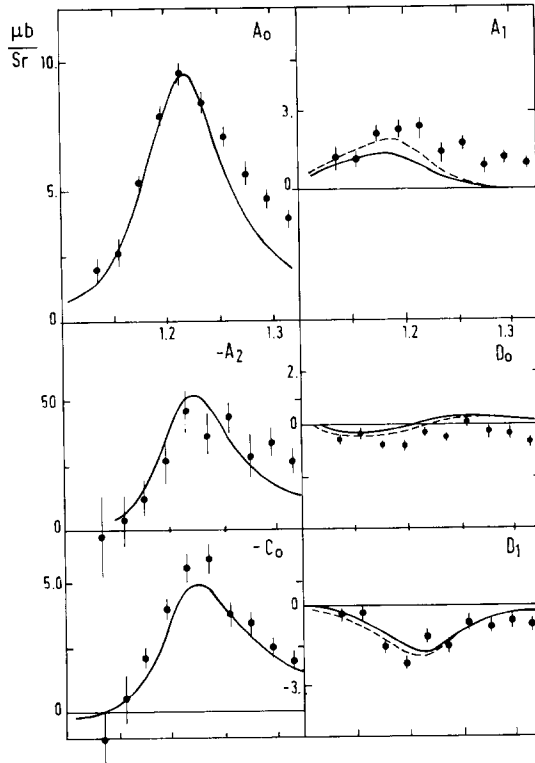
Fig. 1. s and p wave coefficients for $ep \to ep\pi^0$ at $\lambda^2 = -1.0$ GeV^2 in the first resonance region. Data are from ref. [27b]. The full line is fit b using $N + \Delta + s$ wave, the dashed line is the same but including the higher resonances.

δ_{33} phase is well reproduced — at least up to energies just above the resonance position. At higher energies and for $|\lambda^2| > 1.0$ GeV^2 we will see that there is a discrepancy between the fit and the data for $ep \to ep\pi^0$ which can probably be ascribed to a failure to satisfy Watson's theorem exactly. It is well known how to exploit the phase relation by using partial-wave dispersion relations [36] but such a calculation is beyond the scope of the present work*.

The results of the fits to the coincidence data for $ep \to ep\pi^0$ and the peak height data are given in appendix B, table 2. As the peak height data is somewhat model dependent we gave such data a 10% weight relative to the coincidence data. Since the work of Bloom and Gilman [1] there has been a speculation that the P_{33} cross section decreases faster for large λ^2 than the $(\lambda^2)^{-3}$ of the nucleon dipole or of the other resonant peaks. (See also ref. [37].) We have used form factors with asymp-

---

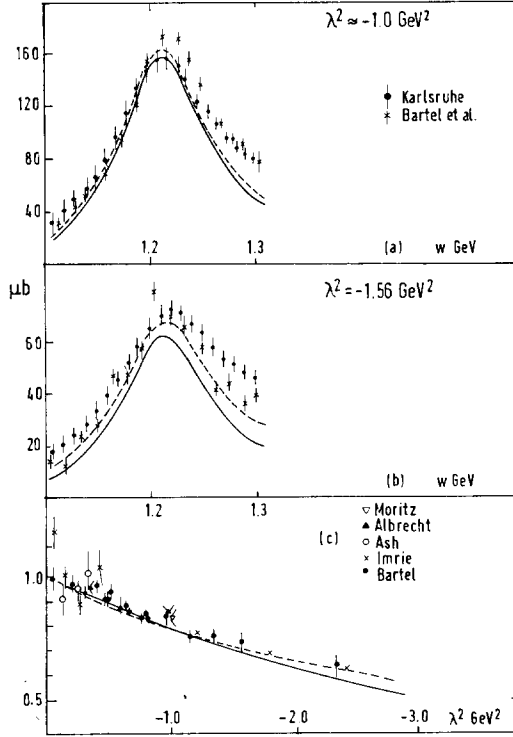* We thank Dr. F. Gutbrod for a discussion on this point.

Fig. 2. (a) and (b) Total cross sections for ep in the first resonance region at $\lambda^2 = -1$ and -1.56 GeV^2. Data are from ref. [45]. The full line is N + Δ + s wave. The dashed line shows the effect of the changes made to F_s and G_E^N described in the text.

(c) $M_{1+}(\lambda^2) \left(M_{1+}(0) \dfrac{k(\lambda^2)}{k(0)} G_{\text{dipole}}(\lambda^2) \right)^{-1}$

The figure is from Gayler [26] and full references to the data are given there. The full line is 1st resonance fit (b), the dashed line fit (a). The crosses show the form factor used in earlier calculations.

totic behaviours of $(\lambda^2)^{-3}$ (fit a) and $(\lambda^2)^{-5}$ (fit b). While the results cannot be said to favour one or the other, the faster decrease does give a slightly better fit to the peak height data. In fig. 1 we show the ep $\rightarrow$ epπ^0 coefficients at $\lambda^2 = -1$ GeV^2. The full line is fit b. The effect of including all the higher resonances from one of our fits is shown by a dashed line. Apart from the coefficient A_1 the effect is almost negligible — justifying our neglect of the higher resonances in the fitting procedure. Fig. 2(c) shows the result for $M_{1+}(\lambda^2)$ compared to "data" for fits (a) and (b). Also shown (by crosses) is the form factor that we used in earlier calculations [3].

    In figs. 2a and 2b we show the calculated total ep cross section from fit (b) compared to data at $\lambda^2 = -1$ and -1.56 GeV^2. It can be seen that the calculation falls

well below the data above the resonance position and is perhaps a little low through-out at $\lambda^2 = -1.56$ GeV^2. Above the resonance about 60% of the discrepancy can be accounted for by the miscalculation of M_{1+} noted above — see also fig. 1 coefficient A_0. What could be responsible for the remaining discrepancy in the charged chan-nel? We know that the effect of the higher resonances is very small (of the order of 3%).

As we discussed earlier two possible sources are G_E^N and the subtraction term. G_E^N is most reliably extracted from ed elastic scattering (subject of course to the usual difficulties of deuterium corrections). The data shows G_E^N to small in the range $0 < |\lambda^2| < 2$ GeV^2 and positive in the range $0 < |\lambda^2| < 0.5$ GeV^2. Beyond 0.5 GeV^2 a change in sign cannot be ruled out. The standard fit to G_E^N that we have used is positive throughout [19]. To increase the cross section it is necessary to change the sign of G_E^N. Obviously the zero must be at $|\lambda^2| \geqslant 0.5$ GeV^2. To indicate the sort of effect on the total cross section we have put a zero at 0.5 GeV by multiplying G_E^N by $(1 + 2 \lambda^2)$. This produces a 6% increase in the cross section at $\lambda^2 = -1.56$ GeV^2. This change is not enough and is probably too drastic a change in G_E^N.

To demonstrate the effect of the subtraction term we have changed the subtrac-tion term form factor F_s from the standard ρ dominance value to a constant (i.e. unity). This produces a 15%–20% increase in the cross section at $\lambda^2 = -1.56$ GeV^2 at energies above the resonance. The result of making both changes simultaneously is shown in fig. 2 by a dashed line.

It is quite conceivable that the subtraction term should have a very slowly de-creasing effective form factor. In our investigation of the subtraction term in ref. [15] we found a cancellation in the t-channel contributions to the integral [eq. (17) above] — assuming identical form factors. The subtraction term can play a role in the total cross section because large t values are reached (of the order of -2.3 GeV^2 at $\lambda^2 = -1.56$ GeV^2). This is not the case for the coincidence data in the channel ep → enπ^+ at the moment. To settle this point the sign of G_E^N at larger λ^2 is needed and coincidence data on ep → enπ^+ at large t and λ^2 will be essential. Al-though G_E^N is best determined from ed scattering something might be learnt from a threshold experiment on ep → enπ^+ at large λ^2*.

Before proceeding to the higher resonance region we must emphasise that the dif-ficulty with the shape of the M_{1+} multipole is only a problem for $|\lambda^2| > 1$ GeV^2.

5.2. Higher resonance region

The resonances included in most of the fits are those shown above the line in table 1, appendix B. In all fits the P_{33} form factor parameters have been fixed at the values obtained in fit (b) in the first resonance region. The reliability of the photoproduction couplings can be judged from table 2 of DLR [6] where a compar-

---

* Our present fit agrees well with the low $|\lambda^2|(<0.3$ GeV^2) threshold results on ep → enπ^+ from NINA [48].

ison is made with other analyses. From there it can be seen that the P_{11}, S_{11}, D_{13}, F_{15} and F_{37} proton couplings are well determined. Apart from the F_{35} the states that have been omitted have very small couplings, and give a very small contribution to $\sigma_{total}(\gamma p)$. We have investigated many fits, the details of some are given in table 3, appendix B, and the χ^2/data point for data blocks are given in table 4, appendix B. For most data the results are in the range 3–4 which is comparable to the quality of fit obtained in photoproduction. The data that is most difficult to fit is the NINA forward π^+n data [28], particularly the forward energy scan. The latter together with other forward π^+n data are shown in fig. 3. As was demonstrated in ref. [28] it is possible to find much better representation of the striking structure seen in this data if one's attention is confined to $\lambda^2 = -0.4$ GeV^2. We have not found it possible to reproduce these results and fit data at other values of λ^2 with the smooth form factors described in sect. 2. The quality of the fit to the distributions at this value of λ^2 is very similar to that reported by Evangelides et al. in ref. [28]. Note also that the failure to fit the low-energy forward points at $\lambda^2 = -0.6$ is not reflected in the fits to the distributions.

The results for the second and thirs peak heights are shown in fig. 4. We have found no difficulty in fitting these data whatever the assumptions made.

Our results for the λ^2 dependence of the multipoles are shown in figs. 5, 6 and 7 (the couplings are all for the ep $\rightarrow$ epπ^0 channel). Here we have tried to show in a direct way which form factors are reasonably well determined and which not. (We have not attempted to determine errors in any conventional way as we do not think

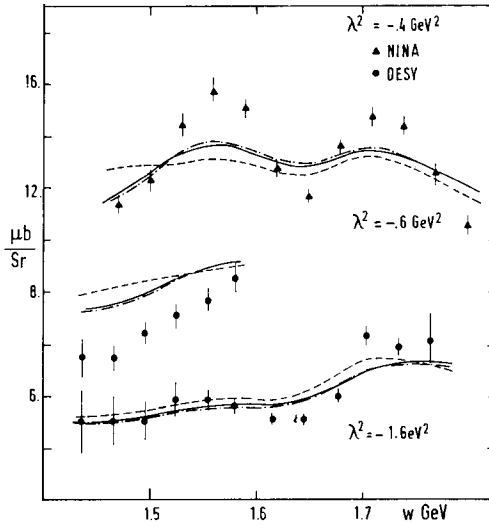Fig. 3. ep $\rightarrow$ enπ^+ forward cross section. Data are from refs. [28,30]. The curves are from various fits to the higher resonance region: full curve fit 1; dashed curve fit 2; dash-dot curve fit 4; see appendix B table 3 for details.
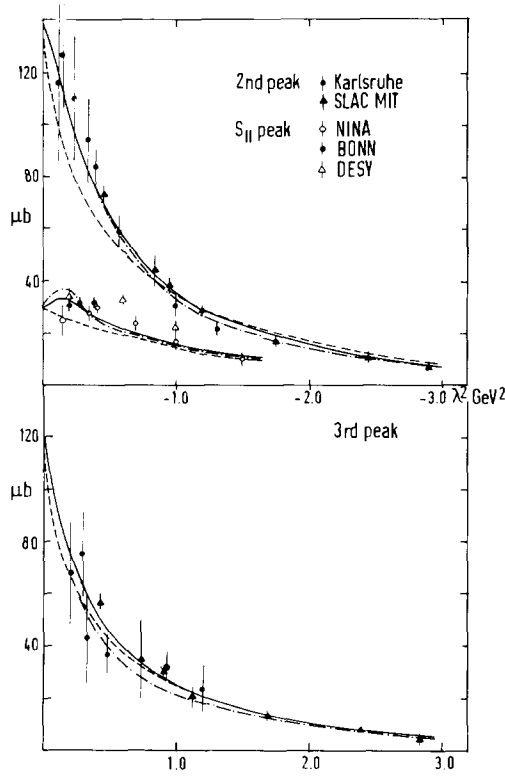
Fig. 4. Second and third peak height data from refs. [25]. Curves as in fig. 3. S_{11} peak data from ref. [35].

it would be very meaningful — what we do try to show is stability against theoretical uncertainty.) The actual parameters for some of the fits can be found in appendix B, table 5.

We find the S_{11}, D_{13}, F_{15} form factors to be stable. The dominant coupling of the F_{37} is also quite stable. In all fits the P_{11} form factor drops extremely fast so that it is effectively absent from the fits to the electroproduction data. This is not too surprising as the structures in the forward $\pi^+ n$ and backward $\pi^0 p$ photoproduction [38] cross sections favouring the P_{11} are not present in electroproduction. Of the smaller photoproduction multipoles the D_{33} and P_{13} are quite well determined. The D_{13}', S_{11}' and D_{13}'' are unstable. Changing the high-energy form factor from ρ dominance to dipole has a very small effect on the results. Likewise putting the subtraction form factor F_s equal to 1 has a small effect. (This can be checked in more detail from table 4 appendix B.) What does produce a significant change in the transverse multipoles and in the fit to the data is the presence or obsence of scalar couplings. The most important scalar coupling is that of the $S_{11}(1505)$. For small
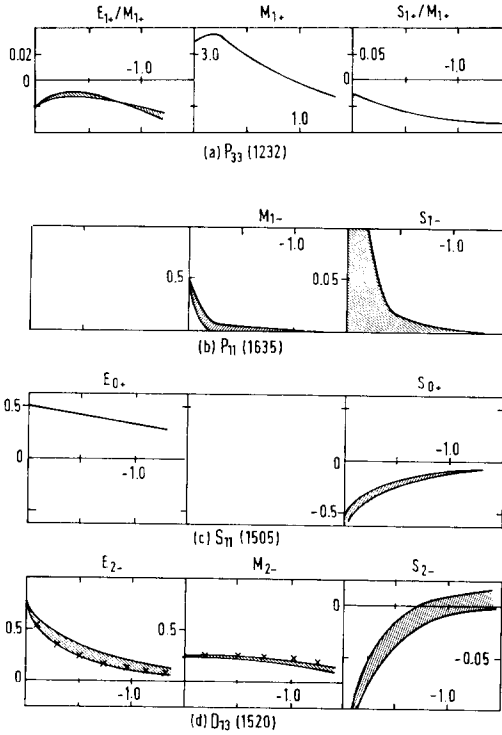
Fig. 5. Multipoles as functions of λ^2 (GeV^2) evaluated at the resonance position. The spread shown is that allowed by the different fits listed in table 3, appendix B. The units are $\mu b^{\frac{1}{2}}$ and the couplings are for the channel ep → epπ^0. The crosses on the graphs for the $D_{13}(1520)$ show the multipoles used in our earlier calculations [3,4], see eq. [20].

λ^2 the ratio σ_s/σ_T can be as large as 40%. Its effect can be seen clearly in figs. 3 and 4. The fit to the S_{11} peak data (deduced from ep → epη) [35] is much improved and so is the fit to the forward π^+n cross section at $\lambda^2 = -0.4$ GeV^2 (table 6, appendix B gives more details of the scalar and transverse peak cross sections for the S_{11}). Of the other resonances most have small scalar couplings except the $D_{13}(1680)$, $D_{33}(1650)$ and $D_{13}{''}(1970)$, which always have essentially zero scalar couplings see figs, 5, 6 and 7. The effect of the scalar couplings when taken together on the resonance peaks produces at most a value of 10% for σ_s/σ_T on the second and third peaks at $\lambda^2 \approx -0.2$ GeV^2 falling to 5% by $\lambda^2 \approx -1.0$ GeV^2. The corresponding figures for the fourth peak are 20% and 6%. These figures are within the limits set by total cross-section data [13]. The results for the F_{15} are noticeably affected by making changes in the composition of the 3rd and 4th peaks (fits 5 and 6). Fit 4 gives the best fit to the coincidence data and we recommend that these parameters be used.

From figs. 5 and 6 it can be seen that the electric multipoles E_{2-} and E_{3-} of the D_{13} and F_{15} respectively fall faster with λ^2 than the corresponding magnetic multi-
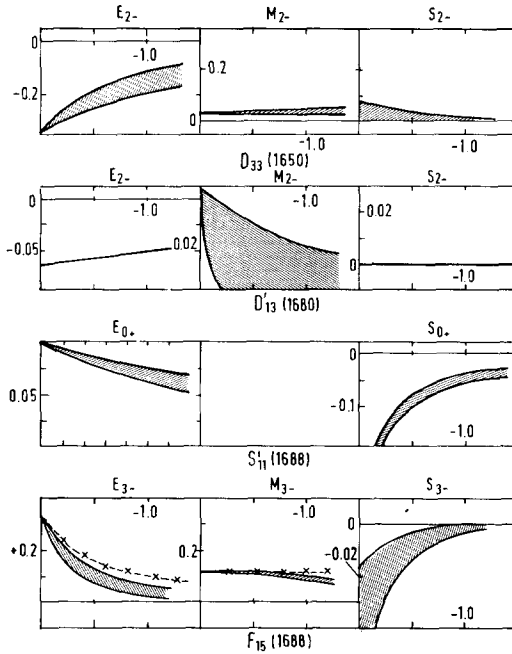
Fig. 6. Multipoles for resonances in the 3rd peak (as fig. 5).
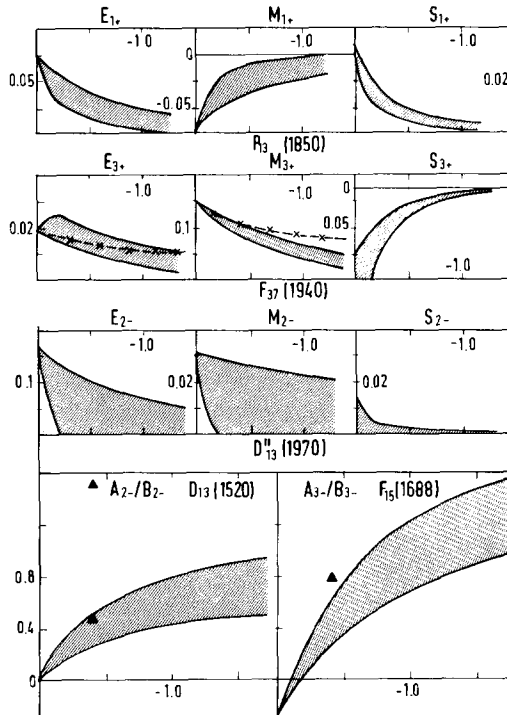

Fig. 7. Multipoles for resonances in the 4th peak (as fig. 5). Ratios A_{2-}/B_{2-}; A_{3-}/B_{3-} for the $D_{13}(1520)$ and $F_{15}(1688)$. ▲ indicates the values from ref. [28] at $\lambda^2 = -0.4$ GeV^2.

poles. This means that the helicity structure of these resonances is changing as a function of λ^2. To show this change more clearly we have drawn the results for the A/B ratio (helicity $\frac{1}{2}$ coupling to helicity $\frac{3}{2}$) for the D_{13} and F_{15} resonances in fig. 7. On this figure we have also indicated the sort of change required to fit the $\pi^+ n$ forward cross section at $\lambda^2 = -0.4$ GeV^2*.

6. Discussion

We have described in some detail how suitable form factors free of kinematical singularities can be choosen for the N* resonances excited in pion electroproduction. We have then shown to what extent such form factors can be determined from existing data. The tool for this investigation has been the fixed-t dispersion relation for the Ball invariant amplitude. Our results for the resonant multipoles as functions of λ^2 are shown in figs. 5–7. (Numerical details are given in appendix B.) In particular we find stable results for the P_{11}, S_{11}, D_{13}, F_{15} and $F_{37}(M_{3+})$. A scalar coupling is found for the S_{11} and to a lesser extent for the D_{13}. It should be remembered that in the absence of separated transverse and scalar cross sections or an accurate measurement of the scalar-transverse interference term the evidence for the scalar contribution is indirect. The principal improvements when non-zero scalar couplings are allowed are in the forward $\pi^+ n$ cross section at $\lambda^2 = -0.4$ (fig. 3) and the 2nd peak and $S_{11}(ep \rightarrow ep\eta)$ peak data (fig. 4). In all cases the results for the scalar cross sections are within the limits set by total cross-section measurements [13]. To give some indication of how our results would compare with our earlier calculations we have shown in figs. 5–7, for the $D_{13}(1520)$, $F_{15}(1688)$ and $F_{37}(1688)$, the form factors obtained from the ansatz

$$G(\lambda^2) = \left| \frac{k(\lambda^2)}{k(0)} \right|^x G_{\text{dipole}} , \qquad (20)$$

where $x = l$ except for E_{l-}, where $x = l - 2$. Although the results are reasonable in the range $0 < |\lambda^2| < 1.0$ GeV^2 the form factors suffer from the serious defect that the resonance contribution to the cross section will have an l dependent λ^2 behaviour namely,

$$\sigma \sim (\lambda^2)^{2(l-2)} , \qquad \text{for large } \lambda^2 .$$

We find that the helicity structure of the $D_{13}(1520)$ and $F_{15}(1688)$ changes quite rapidly with λ^2 (fig. 7). We have also summarized this effect in fig. 8 where we show the helicity asymmetry A calculated on each of the 4 peaks. A is defined by

---

* The results are from ref. [28], but note that the resonance spectrum used there is somewhat different to that used here. For the upper point in fig. 7 ($D_{13}A/B$) zero scalar couplings were used.
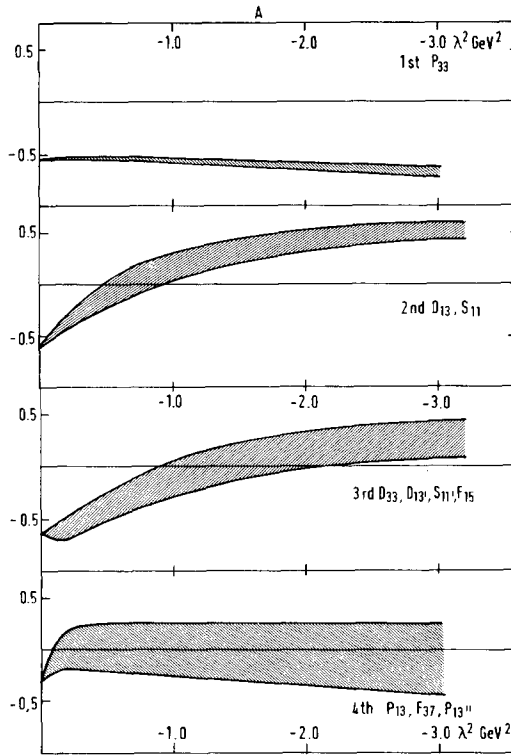
Fig. 8. Helicity asymmetries A evaluated at the peak positions. A is defined by eq. (21). The spread is that allowed by the different fits listed in table 3, appendix B.

$$A = \frac{\sigma_{\frac{1}{2}} - \sigma_{\frac{3}{2}}}{\sigma_{\frac{1}{2}} + \sigma_{\frac{3}{2}}}, \tag{21}$$

where $\sigma_{\frac{1}{2}}$ and $\sigma_{\frac{3}{2}}$ are the total cross sections for helicity $\frac{1}{2}$ and $\frac{3}{2}$ * excitations respectively. The change in sign of the asymmetry could provide some relief for a possible conflict between the quark-parton model (giving $A > 0$) [37] and an extrapolation from photoproduction data (which has $A < 0$) that has recently been emphasised by Close [39]. Note however that some of the change in A shown in fig. 8 comes simply from the fact that the peaks are made from more than one resonance with different helicity structures. In particular in the second peak the S_{11} with positive asymmetry becomes relatively more important as $|\lambda^2|$ increases.

The change in the helicity structure of D_{13} and F_{15} couplings and the well-known absence of change for the P_{33} are in *qualitative* agreement with quark model calculations [40]. Notice however that many quark model calculations find the form factor of the $S_{11}(1505)$ to drop rapidly while that of the $P_{11}(1470)$ stays up in contradic-

tion to the results found here. For a simple calculation in the quark model frame-
work which fits both the D_{13} and S_{11} total cross sections, see Foster [41]. The
changing helicity structure of the D_{13} and F_{15} is also predicted by the B_5 model of
Actor et al. [12].

Apart from the fourth peak and above where there is little or no data very accu-
rate data will be required to improve the determination of the resonance form fac-
tors. In the neutral channel ep $\rightarrow$ epπ^0 the cross section is small of the order of a few
μb/sr. Here the best hope is to increase the θ^* coverage of the data. The present in-
dications are that the scalar contribution is very small. In the charged channel
ep $\rightarrow$ enπ^+ the scalar cross section dominates in the forward direction above the first
resonance region due to pion exchange. Here we have the advantage that resonance
interference effects in the scalar contribution can be enhanced. Even so the scalar-
transverse interference term is still only of the order of 10% of the unseparated cross
section $\sigma_T + \epsilon\sigma_s$. Much bigger effects could be seen in σ_T (up to 50% on the third
peak) if the separation of σ_T and σ_s could be achieved at small θ^* angles. The ques-
tion of the scalar coupling of the S_{11} could well be settled by a forthcoming DESY
experiment to measure σ_T and σ_S in ep $\rightarrow$ epη [42]. Any sort of angular distributions
in the fourth peak region would be helpful.

One final point to note about the way in which we have parametrised the reso-
nance form factors is that because the analytic structure in λ^2 has been respected it
would be possible to use these form factors to estimate resonance production in the
annihilation process $e^+e^- \rightarrow \overline{N}N\pi$, at least near threshold.

We thank the members of the electroproduction group F21 at DESY [34] for
permission to use their data prior to publication. RCED also thanks D. Schiller and
J. Gayler for discussion.

Appendix A

Threshold behaviour and constraints on multipoles

Our basic assumption is that the Ball invariant amplitudes B_i [16] are free of
kinematic singularities in s, t, and λ^2. We require the expression for the multipoles
in terms of the B_i; this is usually given in terms of the Pauli amplitudes, see for ex-
ample ref. [4] appendix A and errata.

We have typically for any multipole

$$M_l = \int_{-1}^{1} dz \sum_i \alpha_i P_{l_i}\phi_i \,, \tag{A.1}$$

---

* Helicity $\frac{1}{2}$ and $\frac{3}{2}$ refer to the possible values of the helicity of the γN system for excitations by
  transversely polarised photons. The total cross section is given by $\sigma = \frac{1}{2}(\sigma_{\frac{1}{2}} + \sigma_{\frac{3}{2}})$.

where α_i are constant coefficients [43], and $\phi_i = X_i F_i$ where F_i are linear combinations of B_i not involving any singularities. The X_i contain square root factors from the spinor wave functions and in particular using

$$E_1 \pm m = \frac{m_\pm^2}{2m^*} \phi_\pm^2 \ ,$$

we find that

$$X_1, X_4, X_7 \sim \phi_+ \qquad \text{as} \qquad \phi_+ \to 0 \ , \tag{A.2}$$

$$X_2, X_3, X_8 \sim \phi_- \qquad \text{as} \qquad \phi_- \to 0 \ . \tag{A.2}$$

Following Jones [44] we assume a fixed s dispersion relation for F_i and insert this into (A.1). Interchanging the order of integration then allows an expression of the form

$$M_l \sim \sum \alpha_i X_i \int_{4\mu^2}^\infty \mathrm{d}t' \ \bar{F}_i(s, t') Q_{l_i}(z') \frac{1}{kq} \ , \tag{A.3}$$

where

$$\bar{F}_i = \mathrm{disc}_t F_i \ .$$

The behaviour as $k \to 0$ we seek will come from the lower and of the integration, using $z' = f(s, t')/kq$ and $Q_l(z') \sim (z')^{-l-1}$ as $z' \to \infty$. Hence

$$M_l \sim \sum \alpha_i X_i k^{l_i} \bar{F}_i \ . \tag{A.4}$$

Given that $k \sim \phi_+ \phi_-$ and knowing the behaviour of the X_i as $\phi_\pm \to 0$ (eq. (A.2)) we can read off the threshold behaviour by looking for the slowest decrease as $\phi_\pm \to 0$. This leads to the results in eqs. (2) and (5).

In the case of α_{l+} one finds that the term involving the slowest decrease as $\phi_+ \to 0$ cancels out of this particular combination. The other combination β_{l+} is choosen for convenience in applying the Macdowell symmetry relations.

To derive the constraints between the scalar and transverse multipoles as $\phi_\pm \to 0$ is a little more complicated. From the invariant amplitude decomposition of the F_i [4] we find as $\phi_+ \to 0$

$$F_7 \to -2m(m^* + m)F_2 + k_0 k_q \cos \theta F_4 \ ,$$

$$F_8 \to k_0 k_q \cos \theta F_3 \ , \tag{A.5}$$

and as $\phi_- \to 0$,

$$F_7 \to k_0 k_q \cos \theta F_4 \ ,$$

$$F_8 \to 2m(m^* - m)F_1 + k_0 k_q \cos\theta \, F_3 \ .$$

These results are inserted into eq. (A.1) for S_l. The combination $\cos\theta \, P_l$ must be re-written using the well-known Legendre function identity before proceeding to eq. (A.4). The constraint then follows from equating the leading terms as $\phi_{\pm} \to 0$ in the expression for E_{l+} and S_{l+}.

The other results follow from Macdowell symmetry, taking account of the fact that M_{l-} will vanish relative to E_{l-} as $\phi_- \to 0$.

Appendix B

Parameters

We give here the quantitative details of the fits to determine the form factors. Table 1 shows the resonance spectrum together with the mass and width parameters used in eq. (14). Also shown are the multipole couplings for the charged photopro-duction channels. The proton peak contribution has been calculated from the $\pi^+ n$ couplings using,

$$\sigma_{l+} = c(l+1)^2 \, \{(l+2)|E_{l+}|^2 + l|M_{l+}|^2\} \ ,$$

$$\sigma_{l-} = cl^2 \, \{(l+1)|M_{l-}|^2 + (l-1)|E_{l-}|^2\} \ , \tag{B.1}$$

where

$$c = \frac{4\pi w_{\mathrm{R}}}{S_{\mathrm{R}} - m^2} \, |q_{\mathrm{R}}| \frac{1}{\eta} ,$$

where

$$\eta^{-1} = \pi N \text{ elasticity} \times \binom{3}{\frac{3}{2}} \text{ for } I = \binom{\frac{3}{2}}{\frac{1}{2}} \ .$$

Tables 2–4 give details of χ^2 results for the fits. Table 5 gives the form factor pa-rameters. The definitions of the form factors and how the parameters enter are shown in sect. 2.

An important point to respect, if amplitudes or cross sections are to be repro-duced, is to use only the parameters from a single fit. The parameters for the badly determined form factors in particular will be highly correlated.

The transverse and scalar peak cross sections for the S_{11} contribution to ep are shown in table 6.

The resonances contributing to the four peaks are as follows; 1st peak P_{33} only; 2nd peak S_{11} and D_{13}; 3rd peak D_{13}', S_{11}', D_{33} and F_{15}; 4th peak P_{13}, F_{37} and D_{13}''.

Table 1

Resonance parameters and photoproduction couplings from DLR [6] η is the πN fraction (see eq. (B.1)) (couplings in $\mu b^{\frac{1}{2}}$; the states below the line have been omitted)

Res	$l_\pm$	W_R, Mass (GeV)	Width (GeV)	η	γp → π⁺n		γn → π⁻p		$\sigma_{\gamma p}^{total}$
					E	M	E	M	
P_{33}	1+	1.232	0.114	0.333	0.4	-2.48	-0.04	2.48	415
P_{11}	1-	1.434	0.2	0.34	—	0.7	—	-0.35	17.4
S_{11}	0+	1.505	0.1	0.21	0.71	—	-0.34	—	30.0
D_{13}	2-	1.514	0.13	0.33	1.02	0.38	-0.64	-0.63	109.0
D_{13}'	2-	1.68	0.128	0.07	-0.1	0.07	-0.1	0.01	8.0
S_{11}'	0+	1.688	0.11	0.07	0.14	—	-0.03	—	3.4
D_{33}	2-	1.649	0.15	0.06	0.24	-0.02	-0.24	0.02	24.0
F_{15}	3-	1.682	0.14	0.35	0.47	0.16	0	-0.08	85.0
P_{13}	1+	1.85	0.3	0.12	0.1	-0.1	0.08	-0.1	10.0
F_{37}	3+	1.94	0.2	0.13	-0.01	-0.11	0.01	0.11	27.0
D_{13}''	2-	1.971	0.427	0.1	0.24	0.05	0.22	0.005	15.0
P_{11}'	1-	1.646	0.142	0.1	—	0.07	—	0.03	0.6
S_{31}	0+	1.66	0.15	0.11	-0.05	—	0.05	—	0.3
P_{33}'	1+	1.75	0.185	0.04	-0.04	-0.02	0.04	0.02	2.5
F_{35}	3-	1.842	0.28	0.05	0.06	0.02	-0.06	-0.02	9.0
P_{31}	1-	1.943	0.2	0.09	—	0	—	0	0.0
D_{15}	2+	1.665	0.175	0.32	0.02	0.06	0.03	-0.2	1.4

Table 2
χ^2/N_{data} for the first resonance region fits (a and b)

Data	λ^2	No	(a)	(b)	(c)	
Coefficient data $ep \to ep\pi°$ [29]	−0.3	30	7.3	7.5	6.6	
	−0.45	36	4.7	4.8	4.3	
	−0.76	30	5.6	5.9	5.4	
	−0.6	48	5.5	5.0	4.6	
	−1.0	60	5.1	5.0	4.2	
	−1.56	27	5.1	4.5	5.3	
Peak height		15	2.6	1.85		
n			3	5	5	

n refers to the asymptotic decrease of the total cross section $\sigma \sim (\lambda^2)^{-n}$. Column c shows the effect of including the higher resonances on fit b.

Table 3
Details of the fits to the higher resonance region; in all cases the P_{33} parameters from fit b were used

Fit	Resonance spectrum	F_H	Scalars = 0	Relative peak/ coincidence weight
1	Standard i.e. all resonances	ρ	no	0.6
2	above the line in table 1 in-	ρ	yes	0.6
3	cluded	dipole	no	0.6
4		ρ	no	0.1
5	Standard + F_{35}	ρ	no	0.1
6	Standard but S_{11}, replaced by D_{15}	ρ	no	0.1

Table 4
χ^2/N_{data} for the data blocks in the higher resonance region, corresponding to the fits listed in table 3

Block χ^2	Ref.	Channel	No	1	1'	2	3	4	5	6	Region (w)
−0.4	[33]	$ep \to ep\pi^0$	131	2.9		2.8	2.9	3.0	2.9	3.1	1.395; 1.575
−0.6	[33,29]		143	2.2		1.9	2.2	2.1	2.1	2.1	1.395; 1.585
−1.0	[29,34]		85	3.1		3.3	2.9	2.4	2.4	2.3	1.345; 1.765
−0.4 (F)	[28]	$ep \to en\pi^+$	14	8.3	8.4	11.1	8.3	8.3	7.5	8.2	1.47; 1.86
−0.4	[28]		116	7.2	7.3	6.7	7.2	7.4	7.6	7.3	1.42; 1.58
−0.6	[30]		76	4.0	3.9	5.2	4.3	3.7	3.6	3.7	1.435; 1.58
−1.0	[30]		204	4.1	4.2	4.4	4.1	3.7	3.7	3.6	1.435; 1.765
−0.3, −0.7	[31, 32]		49	2.6	2.7	3.4	2.4	2.7	2.9	2.8	1.79; 2.05
Peak	[25]		40	0.8		2.1	0.9	1.3	1.5	1.4	

The column labelled 1' shows the effect of changing the subtraction form factor F_s from a ρ pole to unity. The data labelled F is the forward scan at $\lambda^2 = -0.4$ GeV^2.

Table 5
Form factor parameters, units GeV^2; 1 and 2 refer to λ_1^2 and λ_2^2 of eq. (8), a is the scalar parameter [eqs. (10) or (12)]; * indicates parameter fixed; + indicates parameter gives zero scalar coupling [see eq. (11)]

Resonance		(a)	(b)	
	1	0.622	0.43	$\beta_{1+} = \frac{1}{2}(M_{1+} - 3E_{1+})$
	2	0.671	4.715	
P_{33}	1	0.856	0.545	$\alpha_{1+} = \frac{1}{2}(M_{1+} + E_{1+})$
	2	1.28	4.715	
	a	2.7	2.867	see eq. (19) in this case
	n	3	5	$\sigma \sim (\lambda^2)^{-n}$

Resonance		1	2	3	4	5	6	Comment
	M_{1-} 1	0.04	0.11	0.04	0.04			coupling
P_{11}	2	0.041	0.19	0.041	0.041			effectively
	S_{1-} a	0.04	5.628*+	5.628+	0.046			zero
	1	4.08	4.11	4.13	3.63			
S_{11}	E_{0+} 2	4.38	4.46	4.44	4.02	parameters fixed		
	S_{0+} a	0.11	0.32*+	0.12	0.09	as in fit 4		
	1	0.91	0.5	0.79	0.82			
	E_{2-} 2	1.68	1.07	2.01	1.59			
D_{13}	1	0.88	0.98	0.88	0.9			
	M_{2-} 2	1.9	2.19	1.9	1.92			
	S_{2-} a	2.19	0.332*+	2.19	2.19			
	1	2.3	2.37	2.29	1.09	2.05	1.8	
	E_{2-} 2	3.48	3.45	3.47	1.94	2.46	2.4	
D_{33}	1	2.74	2.63	2.77	4.1	3.99	4.44	$M = 10\%$ E
	M_{2-} 2	3.13	3.03	3.07	4.12	4.05	4.89	
	S_{2-} a	6.69+	0.505*+	6.69+	6.69+	6.69+	6.1	
	1	6.85	6.85	6.85	6.85	6.85*	6.85*	
	E_{2-} 2	6.851	6.851	6.851	6.851	6.851*	6.851*	
D_{13}	1	0.04	0.84	0.08	0.04	0.135	0.04	
	M_{2-} 2	0.041	1.88	0.041	0.045	0.16	0.13	
	S_{2-} a	6.85+	0.53*+	6.85+	6.85+	6.85+	6.85+	
	1	3.93	0.04	3.12	5.16	4.14		replaced by
$S_{11'}$	E_{0+} 2	4.03	0.04	3.23	5.18	4.25		D_{15} in 6
	S_{0+} a	0.04	0.55+*	0.04	0.04	0.04		

Table 5 (continued)

Resonance			1	2	3	4	5	6	Comment
	E_{3-}	1	0.59	0.52	0.53	0.53	0.35	0.56	
		2	1.76	1.64	1.73	1.51	1.21	1.32	
F_{15}	M_{3-}	1	1.05	1.13	1.09	1.14	1.06	1.11	
		2	2.87	2.9	2.88	2.98	3.01	2.96	
	S_{3-}	a	5.83	0.553^{*+}	6.2	6.59	6.86^+	4.91	
	β_{1+}	1	0.34	0.77	0.39	0.3	0.28	0.28	
		2	0.63	1.2	0.72	0.43	0.37	0.34	
P_{13}	α_{1+}		Parameters fixed (multipole = 0, at $\lambda^2 = 0$)						
	S_{1+}	a	3.38	0.83^{*+}	3.38	3.34	3.33	3.33	
	β_{3+}	1	0.05	1.39	0.04	0.11	0.1	0.22	
		2	0.051	1.4	0.1	0.43	0.23	0.47	$\beta = 30\%$ M
F_{37}	α_{3+}	1	1.92	1.35	1.85	1.61	1.44	1.55	
		2	3.14	2.75	3.19	4.0	3.98	3.96	
	S_{3+}	a	0.04	1.004^{*+}	0.14	0.04	0.2	0.05	
	E_{2-}	1	0.04	1.55	0.04	0.08	0.17	0.44	
		2	0.041	2.0	0.041	0.25	0.34	0.63	
D_{13}	M_{2-}	1	1.45	0.04	2.08	0.82	0.044	2.14	
		2	2.49	0.04	3.09	2.29	6.34	3.41	
	S_{2-}	a	6.32	1.067^{*+}	8.46^+	8.46^+	8.46^+	8.46^+	

Table 6
The contribution of the $S_{11}(1505)$ to the total ep cross section from fits 1, 2 and 4. (Units are μb)

λ^2	1		2		4	
	σ_T	σ_S	σ_T	σ_S	σ_T	σ_S
−0.15	26.2	7.9	26.3		25.8	11.0
−0.35	22.6	5.0	22.7		21.8	6.5
−0.7	17.8	2.5	17.8	zero	16.6	3.1
−1.0	14.6	1.6	16.7	(fixed)	13.3	1.9
−1.5	10.8	0.9	10.9		9.5	0.9

References

[1] E.D. Bloom and F.J. Gilman, Phys. Rev. D4 (1971) 2901.
[2] A.B. Clegg, Proc. 6th Int. Symp. on electron and photon interactions at high energies, ed. H. Rollnik and W. Pfeil (North Holland, 1974) p. 49.
[3] R.C.E. Devenish and D.H. Lyth, Nucl. Phys. B43 (1972) 228.
[4] R.C.E. Devenish and D.H. Lyth, Phys. Rev. D5 (1972) 47, and errata D6 2067 (1972).
[5] C.N. Brown, C.R. Canizares, W.E. Cooper, A.M. Eisner, G.J. Feldman, C.A. Lichtenstein, L. Litt, W. Locheretz, V.B. Montana and F.M. Pipkin, Phys. Rev. Letters 26 (1971) 991; F.A. Berends, Phys. Rev. D1 2590 (1970).
[6] W.J. Metcalfe and R.L. Walker, Nucl. Phys. B76 (1974) 253;
R.C.E. Devenish, D.H. Lyth and W.A. Rankin, Phys. Letters 52B (1974) 227 (referred to as DLR);
G. Knies, R.G. Moorhouse, H. Oberlack, A. Rosenfeld and A. Rittenberg, reported by D.H. Lyth in Proc. 17th Int. Conf. on high-energy physics 1974, ed. J.R. Smith (Science Research Council, Rutherford Laboratory, 1974) p. II-147;
R.L. Crawford, Glasgow University preprint (1974).
[7] L. Durand, P.C. de Celles and R.B. Marr, Phys. Rev. 126 (1962) 1882.
[8] W.R. Theis and P. Hertel, Nuovo Cimento 66 (1970) 152.
[9] M.D. Scadron and H.F. Jones, Ann. of Phys. 81 (1973) 1.
[10] S.W. MacDowell, Phys. Rev. 116 (1960) 774;
J.S. Ball, Phys. Rev. 124 (1961) 2014.
[11] J.D. Bjorken and J.D. Walecka, Ann. of Phys. 38 (1966) 35.
[12] A. Actor, I. Bender and J. Körner, DESY report (1975).
[13] F.W. Brasse, W. Fehrenbach, W. Flauger, K.H. Frank, J. Gayler, V. Korbel, J. May, P.D. Zimmermann and E. Ganssauge, DESY report No. 71/2, unpublished;
F.W. Brasse, J. of Phys. A5 (1972) 1.
[14] E.M. Riordan, A. Bodek, M. Breidenbach, D.L. Dubin, J.E. Elias, J.E. Friedman, H.W. Kendall, J.S. Poucher, M.R. Sogard and D.H. Coward, Phys. Rev. Letters 33 (1974) 561.
[15] R.C.E. Devenish and D.H. Lyth, Nucl. Phys. B59 (1973) 256.
[16] J.S. Ball, Phys. Rev. 124 (1961) 2014.
[17] A.A. Carter, J.R. Williams, D.V. Bugg, P.J. Bussey and D.R. Dance, Nucl. Phys. B26 (1971) 445.
[18] P. Noelle, W. Pfeil and D. Schwela, Nucl. Phys. B26 (1971) 461.
[19] R. Felst, DESY report No. 73/56.
[20] C. Driver, K. Heinloth, K. Höhne, G. Hofman, P. Karow, D. Schmidt and J. Rathje, Phys. Letters 35B (1971) 770;
C.N. Brown et al., Phys. Rev. Letters 26 (1971) 987 and ref. [5];
C.J. Bebek, C.N. Brown, M. Herzlinger, S. Holmes, C.A. Lichtenstein, F.M. Pipkin, L.K. Sisterson, D. Andrews, K. Berkelman, D.G. Cassel and D.L. Hartill, Phys. Rev. D9 (1974) 1229.
[21] T. Azemoon, D. Lüke, G. Specht, H. Ackermann, E. Ganssauge, F. Janata and D. Schmidt, DESY report No. 74/46.
[22] G.F. Chew, M.L. Goldberger, F.E. Low and Y. Nambu, Phys. Rev. 106 (1957) 1345.
[23] C.F. Cho and J.J. Sakurai, Phys. Rev. D2 (1970) 519;
B.H. Kellett, Nucl. Phys. B38 (1972) 573.
[24] P. Stichel, Z. Phys. 180 (1964) 170;
G. Kramer, Acta Phys. Austriaca 40 (1974) 150.
[25] M. Breidenbach, Thesis M.I.T. Report No. 2098-635 (1970) unpublished;
M. Köbberling, J. Moritz, K.H. Schmidt, D. Wegener, D. Zeller, J. Bleckwenn and F.H. Heimlich, Nucl. Phys. B82 (1974) 201.

[26] J. Gayler, Daresbury Study Weekend on inelastic electron scattering, 1971, DNPL R/15, ed. A. Donnachie.

[27] (a) R. Siddle, B. Dickinson, M. Ibbotson, R. Lawson, H.E. Mongomery, V.P.R. Nuthakki, O.T. Tumer, W.J. Shuttleworth, A. Sofair, R.D. Hellings, J. Allison, A.B. Clegg, F. Foster, G. Hughes, P.S. Kummer and J. Fannon, Nucl. Phys. B35 (1971) 93.
(b) J.C. Alder, F.W. Brasse, E. Chazelas, W. Fehrenbach, W. Flauger, K.H. Frank, E. Ganssauge, J. Gayler, V. Korbel, J. May, M. Merkwitz, A. Courau, G. Tristram and J. Valentin, Nucl. Phys. B46 (1972) 573.

[28] E. Evangelides, R. Meaburn, J. Allison, B. Dickinson, M. Ibbotson, R. Lawson, H.E. Montgomery, D. Baxter, F. Foster, G. Hughes, P.S. Kummer, R. Siddle, D.H. Lyth and R.C.E. Devenish, Nucl. Phys. B71 (1974) 381.

[29] J.C. Alder, H. Behrens, F.W. Brasse, W. Fehrenbach, J. Gayler, V. Korbel, W. Krechlok, J. May and M. Merkwitz, paper No. 156 presented to the 6th Int. Symp. on electron and photon interactions at high energies, Bonn, 1973. reported in ref. [2].

[30] H. Behrens, Diplomarbeit Fachbereich Physik der Universität Hamburg 1974, unpublished.

[31] C.N. Brown et al., ref. [20] and ref. [5].

[32] P.S. Kummer, A.B. Clegg, F. Foster, G. Hughes, R. Siddle, J. Allison, B. Dickinson, E. Evangelides, M. Ibbotson, R. Lawson, R.W. Meaburn, H.E. Montgomery, W.J. Shuttleworth and A. Sofair, Nuovo Cimento Letters 1 (1971) 1026.

[33] W.J. Shuttleworth, A. Sofair, R. Siddle, B. Dickinson, M. Ibbotson, R. Lawson, H.E. Montgomery, R.D. Hellings, J. Allison, A.B. Clegg, F. Foster, G. Hughes and P.S. Kummer, Nucl. Phys. B45 (1972) 428.

[34] J.C. Alder, H. Behrens, F.W. Brasse, W. Fehrenbach, J. Gayler, R. Haidan, S.P. Goel, V. Korbel, J. May and M. Merkwitz, private communication, to be published summer 1975.

[35] P.S. Kummer, E. Ashburner, F. Foster, G. Hughes, R. Siddle, J. Allison, B. Dickinson, E. Evangelides, M. Ibbotson, R.S. Lawson, R.S. Meaburn, H.E. Montgomery and W.J. Shuttleworth, Phys. Rev. Letters 30 (1973) 873;
U. Beck, K.H. Becks, V. Burkert, J. Drees, B. Dresbach, B. Gerhardt, G. Knop. H. Kolanoski, M. Leenen, K. Moser, H. Müller, Ch. Nietzel, J. Päsler, K. Rith, M. Rosenberg, R. Sauerwein, E. Schlösser and H.E. Stier, Phys. Letters 51B (1974) 103;
J.C. Alder, F.W. Brasse, W. Fehrenbach, J. Gayler, R. Haidan, G. Glöe, S.P. Goel, V. Korbel, W. Krecklok, J. May, M. Merkwitz, R. Schmitz and W. Wagner, DESY report No. 74/61.

[36] G. von Gehlen, Nucl. Phys. B20 (1968) 102;
R.L. Crawford, Nucl. Phys. B28 (1971) 573.

[37] B. Flume-Gorczyca and S. Kitakado, DESY report No. 74/48.

[38] R.C.E. Devenish, D.H. Lyth and W.A. Rankin, Phys. Letters 36B (1971) 394.

[39] F.E. Close, CERN-TH-1843 talk given at the 9th Rencontre de Moriond 1974, to be published.

[40] F. Ravndal, Phys. Rev. D4 (1971) 1466;
L.A. Copley, G. Karl and E. Obryk, Phys. Rev. D4 (1971) 2844;
R.G. Lipes, Phys. Rev. D5 (1972) 2849;
T. Abdullah and F.E. Close, Phys. Rev. D5 (1972) 2332.

[41] F. Foster, Proc. of the London Conf., 1974, see ref. [6] p. II-163.

[42] DESY proposal No. 134. F21 group approved to run in 1975.

[43] N. Zagury, Phys. Rev. 145 (1966) 1112.

[44] H.F. Jones, Nuovo Cimento 40A (1965) 1018.

[45] W. Bartel, B. Dudelzak, H. Krehbiel, J. McElroy, U. Meyer-Berkhout, W. Schmidt, V. Walther and G. Weber, Phys. Letters 28B (1968) 148;
K. Köbberling et al., Karlsruhe Report K.F.K. 1822, 1973 (unpublished) and ref. [27].

[46] R.L. Walker, Phys. Rev. 182 (1960) 1729.

[47] K. Berkelman, 1971 Int. Symposium on electron and photon interactions at high energies, ed. K. Mistry, Cornell University, 1972.

[48] P. Norton, Private communication, Daresbury Laboratory PEP group, forthcoming report.